In vivo volumetric imaging of the human corneo-scleral limbus with spectral domain OCT

Kostadinka Bizheva,[1,*] Natalie Hutchings,[2] Luigina Sorbara,[2] Alireza A. Moayed,[1] and Trefford Simpson[2]

[1]*Department of Physics and Astronomy, University of Waterloo, 200 University Avenue West, Waterloo, ON N2L3G1, Canada*

[2]*School of Optometry, University of Waterloo, 200 University Avenue West, Waterloo, ON N2L3G1, Canada*

**kbizheva@uwaterloo.ca*

Abstract: The limbus is the structurally rich transitional region of tissue between the cornea on one side, and the sclera and conjunctiva on the other. This zone, among other things, contains nerves passing to the cornea, blood and lymph vasculature for oxygen and nutrient delivery and for waste, CO_2 removal and drainage of the aqueous humour. In addition, the limbus contains stem cells responsible for the existence and healing of the corneal epithelium. Here we present 3D images of the healthy human limbus, acquired *in vivo* with a spectral domain optical coherence tomography system operating at 1060nm. Cross-sectional and volumetric images were acquired from temporal and nasal locations in the human limbus with ~3μm x 18μm (axial x lateral) resolution in biological tissue at the rate of 92,000 A-scans/s. The imaging enabled detailed mapping of the corneo-scleral tissue morphology, and visualization of structural details such as the Vogt palisades, the blood and lymph vasculature including the Schlemm's canal and the trabecular meshwork, as well as corneal nerve fiber bundles. Non-invasive, volumetric, high resolution imaging reveals fine details of the normal human limbal structure, and promises to provide invaluable information about its changes in health and disease as well as during and after corneal surgery.

OCIS codes: (170.4500) Optical coherence tomography; (170.0110) Imaging systems; (170.3880) Medical and biological imaging; (170.4470) Ophthalmology;

References and links

1. D. M. Maurice, "The structure and transparency of the cornea," J. Physiol. **136**(2), 263–286 (1957).
2. K. M. Meek and N. J. Fullwood, "Corneal and scleral collagens--a microscopist's perspective," Micron **32**(3), 261–272 (2001).
3. E. B. Papas, "The limbal vasculature," Cont. Lens Anterior Eye **26**(2), 71–76 (2003).
4. J. G. Lawrenson and G. L. Ruskell, "The structure of corpuscular nerve endings in the limbal conjunctiva of the human eye," J. Anat. **177**, 75–84 (1991).
5. J. G. Lawrenson and G. L. Ruskell, "Investigation of limbal touch sensitivity using a Cochet-Bonnet aesthesiometer," Br. J. Ophthalmol. **77**(6), 339–343 (1993).
6. D. J. Spalton, R. A. Hitchings, and P. A. Hunter, *Clinical Ophthalmology* (Lippincott, Philadelphia, 1984).
7. A. J. Bron, "Vortex patterns of the corneal epithelium," Trans. Ophthalmol. Soc. U. K. **93**(0), 455–472 (1973).
8. M. F. Goldberg and A. J. Bron, "Limbal palisades of Vogt," Trans. Am. Ophthalmol. Soc. **80**, 155–171 (1982).
9. W. M. Townsend, "The limbal palisades of Vogt," Trans. Am. Ophthalmol. Soc. **89**, 721–756 (1991).
10. H. S. Dua and A. Azuara-Blanco, "Limbal stem cells of the corneal epithelium," Surv. Ophthalmol. **44**(5), 415–425 (2000).
11. D. V. Patel, T. Sherwin, and C. N. McGhee, "Laser scanning *in vivo* confocal microscopy of the normal human corneoscleral limbus," Invest. Ophthalmol. Vis. Sci. **47**(7), 2823–2827 (2006).
12. P. B. Thomas, Y. H. Liu, F. F. Zhuang, S. Selvam, S. W. Song, R. E. Smith, M. D. Trousdale, and S. C. Yiu, "Identification of Notch-1 expression in the limbal basal epithelium," Mol. Vis. **13**, 337–344 (2007).
13. L. Oliveira-Soto and N. Efron, "Morphology of corneal nerves using confocal microscopy," Cornea **20**(4), 374–384 (2001).
14. D. Huang, E. A. Swanson, C. P. Lin, J. S. Schuman, W. G. Stinson, W. Chang, M. R. Hee, T. Flotte, K. Gregory, C. A. Puliafito, and J. G. Fujimoto, "Optical coherence tomography," Science **254**(5035), 1178–1181 (1991).

#143753 - $15.00 USD Received 7 Mar 2011; revised 27 May 2011; accepted 31 May 2011; published 1 Jun 2011

15. A. F. Fercher, "Optical coherence tomograohy," J. Biomed. Opt. **1**(2), 157–999 (1996).
16. V. Christopoulos, L. Kagemann, G. Wollstein, H. Ishikawa, M. L. Gabriele, M. Wojtkowski, V. Srinivasan, J. G. Fujimoto, J. S. Duker, D. K. Dhaliwal, and J. S. Schuman, "*In vivo* corneal high-speed, ultra high-resolution optical coherence tomography," Arch. Ophthalmol. **125**(8), 1027–1035 (2007).
17. M. V. Sarunic, S. Asrani, and J. A. Izatt, "Imaging the ocular anterior segment with real-time, full-range Fourier-domain optical coherence tomography," Arch. Ophthalmol. **126**(4), 537–542 (2008).
18. J. Jungwirth, B. Baumann, M. Pircher, E. Götzinger, and C. K. Hitzenberger, "Extended *in vivo* anterior eye-segment imaging with full-range complex spectral domain optical coherence tomography," J. Biomed. Opt. **14**(5), 050501 (2009).
19. M. Gora, K. Karnowski, M. Szkulmowski, B. J. Kaluzny, R. Huber, A. Kowalczyk, and M. Wojtkowski, "Ultra high-speed swept source OCT imaging of the anterior segment of human eye at 200 kHz with adjustable imaging range," Opt. Express **17**(17), 14880–14894 (2009).
20. Y. Feng and T. L. Simpson, "Comparison of human central cornea and limbus *in vivo* using optical coherence tomography," Optom. Vis. Sci. **82**(5), 416–419 (2005).
21. M. Singh, T. Aung, D. S. Friedman, C. Zheng, P. J. Foster, W. P. Nolan, J. L. See, S. D. Smith, and P. T. K. Chew, "Anterior segment optical coherence tomography imaging of trabeculectomy blebs before and after laser suture lysis," Am. J. Ophthalmol. **143**(5), 873–875 (2007).
22. T. Theelen, P. Wesseling, J. E. E. Keunen, and B. J. Klevering, "A pilot study on slit lamp-adapted optical coherence tomography imaging of trabeculectomy filtering blebs," Graefes Arch. Clin. Exp. Ophthalmol. **245**(6), 877–882 (2007).
23. L. Kagemann, G. Wollstein, H. Ishikawa, R. A. Bilonick, P. M. Brennen, L. S. Folio, M. L. Gabriele, and J. S. Schuman, "Identification and assessment of Schlemm's canal by spectral-domain optical coherence tomography," Invest. Ophthalmol. Vis. Sci. **51**(8), 4054–4059 (2010).
24. A. Miyazawa, M. Yamanari, S. Makita, M. Miura, K. Kawana, K. Iwaya, H. Goto, and Y. Yasuno, "Tissue discrimination in anterior eye using three optical parameters obtained by polarization sensitive optical coherence tomography," Opt. Express **17**(20), 17426–17440 (2009).
25. N. Hutchings, T. L. Simpson, C. Hyun, A. A. Moayed, S. Hariri, L. Sorbara, and K. Bizheva, "Swelling of the human cornea revealed by high-speed, ultrahigh-resolution optical coherence tomography," Invest. Ophthalmol. Vis. Sci. **51**(9), 4579–4584 (2010).
26. Y. Wang, J. Nelson, Z. Chen, B. Reiser, R. Chuck, and R. Windeler, "Optimal wavelength for ultrahigh-resolution optical coherence tomography," Opt. Express **11**(12), 1411–1417 (2003).
27. "Anatomy of the human eye," *http://www.images.missionforvisionusa.org/anatomy/2005/10/cornea-histology.html*.
28. *http://www.bu.edu/histology/p/08005loa.htm*, Reproduced with permission from Prof. Deborah W. Vaughan.
29. T. Tervo and A. Palkama, "Ultrastructure of the corneal nerves after fixation with potassium permanganate," Anat. Rec. **190**(4), 851–859 (1978).

1. Introduction

The limbus is the transitional tissue from the cornea to the conjunctiva and sclera, approximately 1.5 mm wide in adult human eyes, that has rich structural variation, with organizational alteration—from scleral irregular opacity to corneal regularity and transparency [1,2], vascular variation within the conjunctiva, sclera and peripheral cornea [3], and neural passage and termination [4,5]. The limbus is also the common site for the occurrence of early corneal neovascularization, phlyctenulosis and other limbal follicles, lupus vulgaris and corneal epithelium neoplasia [6]. These diseases can cause morphological changes in the limbus that cannot be observed non-invasively in 3D with currently existing clinical instrumentation. The human limbus contains radially oriented fibrovascular ridges, connecting the cornea and the bulbar conjunctiva, known as the palisades of Vogt [7]. The regions between the ridges of the Vogt palisades have been shown to house corneal stem cells, which play a key role in the regeneration of the corneal epithelium [8–10]. Currently, slit-lamps are used for clinical examination of the limbal morphology, however, this technology does not allow for volumetric, high resolution imaging of structural details. Recently, cellular level resolution images of the human corneo-scleral limbus were obtained *in vivo* with commercial laser scanning confocal microscopes (LSCM), that showed detailed 2D en-face view of the Vogt palisades [11,12]. Similar studies were carried out to image *in vivo* nerves and nerve fiber bundles in the human cornea and limbus and provide thorough classification of the nerves in terms of size, shape, reflectivity and position in the cornea [13]. Although the quality of these images is impressive, there are a few disadvantages to using LSCM for corneal and limbus imaging: a) the measurement procedure is invasive, i.e., requires physical contact between the LSCM imaging probe and the corneal epithelium or conjunctiva; b) since the LSCM field of view is small (~200μm x 200μm), a 2D view of ~1mm x 1mm area of the

#143753 - $15.00 USD Received 7 Mar 2011; revised 27 May 2011; accepted 31 May 2011; published 1 Jun 2011

corneo-scleral limbus requires acquisition and "stitching" of multiple, typically more than 10, LSCM images, thus increasing significantly the image acquisition and processing time; and c) due to the limited LSCM axial resolution, volumetric visualization of the limbus morphology is not trivial.

Optical coherence tomography (OCT) is an imaging modality that allows for non-invasive imaging of the morphology of biological tissue with micrometer scale resolution at imaging depths of 1-2mm below the tissue surface [14,15]. Because of the transparency of the eye, the posterior segment (retina) is also readily accessible using OCT. Over the past decade, commercial and research ultrahigh resolution OCT (UHROCT) systems have been used in ophthalmology to acquire non-invasively and *in vivo* high resolution images of the human ocular anterior segment, and specifically, the cornea [16–19]. However, very few studies have focused on using OCT technology for morphological imaging of the limbus, sclera and conjunctiva [10–22]. In all of these studies the axial OCT resolution was limited to ~10μm, which prevented visualization of fine morphological details in the limbal and scleral tissue. Recently, an UHROCT system operating at ~800nm with axial resolution of ~3μm in biological tissue was used for *in vivo* identification and assessment of the Schlemm's canal [23], while a different study used polarization sensitive UHROCT operating to identify the trabecular meshwork (TM) [24].

Here we present high resolution, cross-sectional and volumetric images of the human corneo-scleral limbus, acquired with a high speed, spectral domain UHROCT system, that allow for visualization of morphological details such as the Vogt palisades, corneal nerve bundles, the Schlemm's canal and TM, as well as the limbal and scleral blood and lymph vasculature.

2. Methods

A high speed spectral domain UHROCT system operating at ~1060nm was developed for *in vivo* imaging of the human anterior chamber and recently applied in a study of hypoxia-induced corneal swelling in human subjects [25]. When applied to imaging the anterior structures of the human eye, any UHROCT system operating in the 1060nm spectral range has a major advantage over similar systems operating at 800nm or 1300nm [26]: if dispersion within the imaging system is perfectly balanced, the acquired images do not require post-processing for water dispersion compensation, since water has a dispersion null in the 1μm spectral region. Briefly, the UHROCT system used in this study is based on a compact, fiber-optic Michelson interferometer, connected to a broad bandwidth superluminescent diode, SLD (Superlum Ltd., λ_c = 1020 nm, $\Delta\lambda$ = 110 nm, P_{out} = 9 mW). The reference arm is comprised of an achromatic collimator (Edmund Optics), a custom tunable dispersion compensation unit based on a pair of BK7 glass prisms, a focusing achromatic lens and an Ag mirror mounted on a translation stage. The sample arm of the system consists of an optical imaging probe, mounted on a modified slit lamp biomicroscope. The imaging probe is comprised of 3 achromatic doublet lenses (Edmund Optics, f_1 = 20mm, f_2 = f_3 = 35mm) and a pair of galvanometric scanners (Cambridge Technologies). The interference signal is detected with a custom, high performance spectrometer (P&P Optica), interfaced to a 1024 pixel linear array InGaAs camera (SUI, Goodrich Corp.) with 92 kHz readout rate. The UHROCT system and imaging interface provide 3μm axial and 18μm lateral resolution in biological tissue and depth of focus of ~250 μm (Rayleigh range). The axial OCT resolution degrades only by ~10% over the entire scanning range due to fringe washout. Because the cornea scatters light weekly and the water absorption in the cornea over the pathlength of ~1.2mm (double pass in a human cornea with total average thickness of ~600 μm) has minimal effect on the spectral bandwidth of the light source used, the axial resolution is fairly constant over the entire depth of the OCT images. The lateral resolution varies from 18 μm at the focal plane to ~35μm at the anterior and posterior ends of the cornea when the focal plane is located in the central stroma. The UHROCT system also provides ~96dB SNR for 1.5mW power of the imaging beam. All tomograms were processed with Matlab (Mathworks) and Amira (Visage Imaging).

#143753 - $15.00 USD Received 7 Mar 2011; revised 27 May 2011; accepted 31 May 2011; published 1 Jun 2011

UHROCT tomograms were acquired *in vivo* from the corneo-scleral limbus of two human subjects. The imaging procedure was approved by the Human Ethics Committee at the University of Waterloo. The subjects were pre-screened to ensure that there were no anterior eye health issues (e.g. active inflammation or dry eye) that contraindicated the imaging procedure. In both subjects the limbus had a clinically normal appearance (observed using slit lamp biomicroscopy). During the imaging procedure each subject placed their head on a chin-forehead support frame and an external fixation light was used to position the eyes of the subject so that the nasal or temporal part of the limbus was centered in the tomogram. 3D stacks of UHROCT tomograms (1000 A-scans x 1024 Pixels in depth x 256 B-scans), corresponding to 5mm x 1mm x 2.5mm were acquired from the nasal and temporal limbus. The acquisition time for each 3D image stack was 2.8 seconds. Because of motion artifacts associated with natural eye motion during the imaging procedure, the edges of the 3D image stacks were trimmed by ~10% resulting in effective en-face imaged area of 4mm x 2mm.

3. Results and discussion

Figure 1A shows a representative 2D UHROCT tomogram of the healthy human corneo-scleral limbus acquired from a temporal location. The major corneal layers such as the epithelium (Ep), Bowman's membrane (BM), stroma (S) and the Descemet's – Endothelium complex (DEC) are visible on the left (corneal) side of the tomogram. Longitudinal and normal cross-sections of structural features resembling blood or lymph vessels are observed in the limbal (right) side of the image (red arrows). Because the ranges of vessel diameter and flow velocities in the blood and lymph vessels can overlap, structural and Doppler OCT cannot be used alone to differentiate between blood and lymph vessels in the limbus. Spectroscopic analysis that can utilize the wavelength dependent scattering and absorption properties of blood and lymph, maybe helpful in future studies that target to differential lymph from blood vasculature in the human corneo-scleral limbus. The limbus is also the location where the corneal epithelium transitions into the bulbar conjunctival epithelium, the most superficial layer of the transparent tissue overlying the white sclera. The image in Fig. 1A shows differences in the structure and optical properties of the corneal epithelium and the bulbar conjunctiva that can be associated with difference in the tissue morphology. While the corneal epithelium (blue arrow) appears more transparent, the conjunctiva (green arrow) appears more optically scattering (darker shade of gray color). A magnified view of the region in the corneal epithelium, marked with the red square in Fig. 1A, is presented in Fig. 1B and

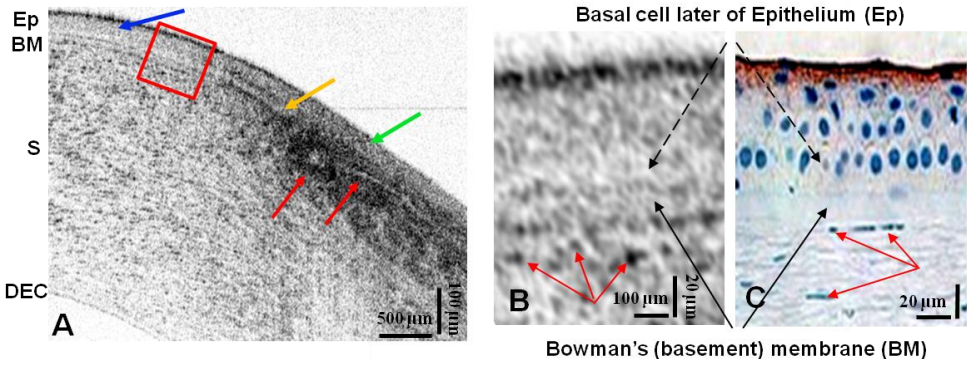

Fig. 1. A representative cross-sectional UHROCT tomogram of the human corneo-scleral limbus acquired from a temporal location (A). The blue arrow marks the corneal epithelium; the orange, the termination of the basal cell layer of the corneal epithelium in the limbus; the green, the bulbar conjunctiva; and the red, limbal blood or lymph vessels. 1B is a magnified view of the corneal epithelium marked with the red square in 1A. 1C shows a representative histology of the healthy human cornea [27]. Black dashed arrows in 1B and 1C mark the basal cell layer of the corneal epithelium, solid black arrows mark the Bowman's membrane, and red arrows mark the nuclei of keratocyte cells in the corneal stroma.

#143753 - $15.00 USD Received 7 Mar 2011; revised 27 May 2011; accepted 31 May 2011; published 1 Jun 2011

compared with a representative histological cross-section [27] (Fig. 1C). The Bowman's membrane boundaries are visible in Fig. 1A and in Fig. 1B (black solid arrows) and its thickness (~15 μm) compares well with the histological cross-section. Furthermore, a low reflective band is visible at the interface between the corneal epithelium and the Bowman's membrane both in the original image (Fig. 1A) and the magnified view (Fig. 1B, dashed black arrows). Comparison with histology (Fig. 1C) suggests that the band most likely corresponds to the basal cell layer of the corneal epithelium, comprised of columnar cells that are ~15μm to 20μm in length. Corneal basal epithelial cells have a large cytoplasm to nucleus ratio, which explains the lower scattering of this cell layer as compared to the upper epithelial layers. Figure 1A also shows the termination of the corneal epithelium basal layer in the limbus (orange arrow). Upper layers of the corneal epithelium were not individually resolved due to the smaller axial dimensions of the polyhedral and squamous cells comprising those layers, which are comparable to the 3μm axial resolution of the current UHROCT system.

Figure 2 shows comparison between histology [28] of the human corneo-scleral limbus (A) and a representative UHROCT tomogram of the human temporal limbus acquired *in vivo* from a nasal location (B). The 3μm axial resolution of the UHROCT system is not sufficient to resolve the endothelium (En) and the Descemet's membrane however a combination of the two layers is observed that we refer to as the Descemet's Endothelium Complex (DEC) that can be distinguished from the corneal stroma (S). The high axial resolution of the optical imaging system also allows for clear visualization of the Schlemm's canal (white arrows) and the trabecular meshwork (TM) (black arrows).

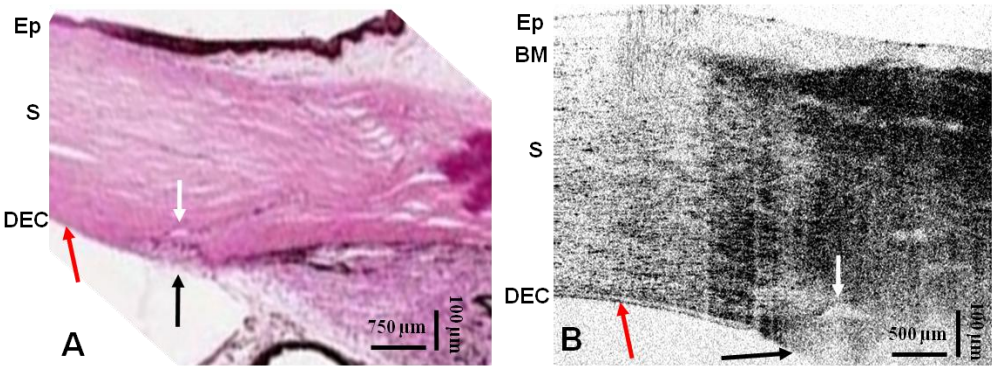

Fig. 2. Comparison between H&E histology of the human corneal limbus [28] (A) and a representative UHROCT tomogram of the human temporal limbus acquired *in vivo* (B). Red arrows mark at the corneal endothelium, white arrows the Schlemm's canal, and black arrows the trabecular meshwork (TM).

Multiple 3D stacks of UHROCT images were acquired from temporal and nasal locations in the eye in all subjects. Figure 3 shows representative 2D tomograms of healthy, normal human limbus, acquired temporally (A-D) and nasally (E, F). The left side of the tomograms in Figs. 3 A-F show the cornea, where the corneal layers are clearly visualized. The right side of the same images shows the highly scattering sclera with networks of blood and lymph vessels. The corneal epithelium and the bulbar conjunctiva are marked with blue and green arrows respectively. Figure 3B shows another representative temporal scan of the limbus from the same subject. A highly reflective (dark grey color) fork-like feature, 15μm in diameter (inside the red rectangle) is clearly visible in the corneal region of the tomogram. According to a recent *in vivo* study of the cornea conducted with a confocal microscope [13], the size (~15μm diameter), location (mid stroma), shape (almost straight line with a bifurcating end) and high reflectivity of this structure suggests that it most likely corresponds to a corneal nerve fiber bundle. Notice that the feature extends well into sclera region of the tomogram (red arrow), but its appearance (color) changes from dark grey to almost white in the tomogram. This change is perhaps due to the fact that corneal tissue is far less scattering than

#143753 - $15.00 USD Received 7 Mar 2011; revised 27 May 2011; accepted 31 May 2011; published 1 Jun 2011

the nerve fibers, therefore in the corneal part of the UHROCT tomogram, a nerve fiber bundle will appear dark grey in color. However, scleral tissue is highly scattering, therefore a nerve fiber bundle, which is less scattering than the scleral tissue, would appear in pale grey color in the scleral part of the UHROCT tomogram. Alternatively, the change in the apparent reflectivity of the nerve fiber bundle can be manifestation of the change in the nerve itself, since nerves lose their myelin sheaths as they transition into the cornea [29].

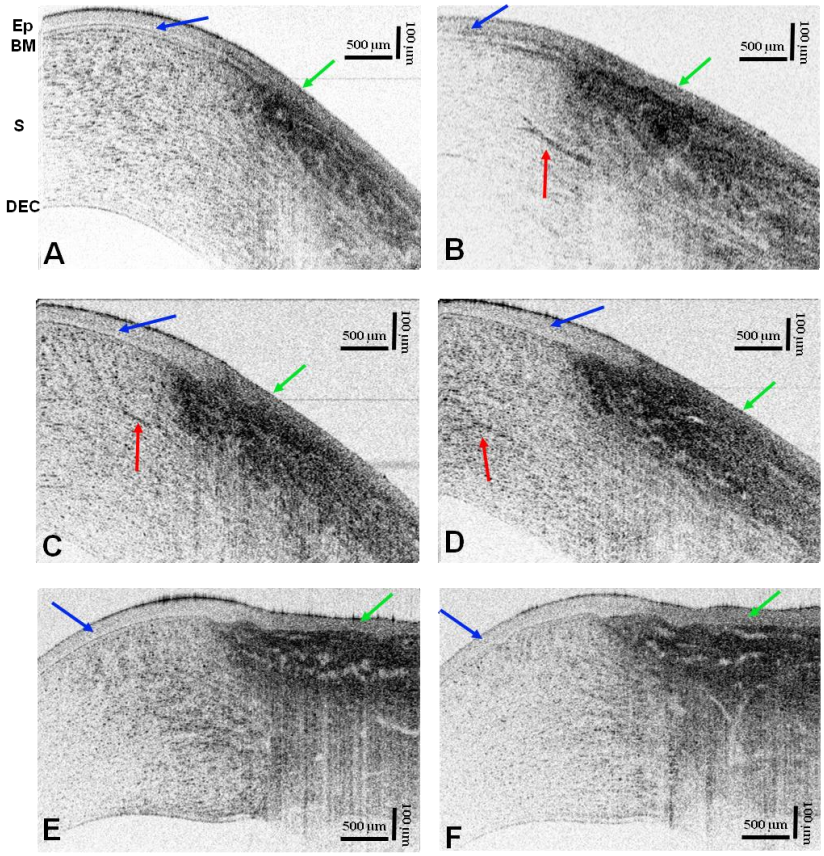

Fig. 3. Representative UHROCT tomograms of the normal human limbus acquired *in vivo* from temporal (A-D) and nasal (E,F) locations. Blue and green arrows mark the cornea and the bulbar conjunctiva, respectively. Red arrows mark corneal nerves.

To highlight subject-related differences in the morphology and optical properties of the limbal tissue as imaged with UHROCT, representative temporal UHROCT images of the limbus of the second subject are shown (Figs. 3C, D). In general, the limbus structure appears similar in both cases; however, the difference in the optical properties of the corneal epithelium and the bulbar conjunctiva, as well as the transition between these two tissues appears more pronounced in the second illustration. Furthermore, a number of finer nerve fibre bundles are visible in Fig. 3C (red arrows) and Fig. 3D, which appear thinner (~10µm in diameter) than the nerve fibre observed in subject one (Fig. 3B). Representative nasal scans of the limbus acquired from subject number two are shown in Figs. 3E, F. Morphologically, the temporal and nasal scans appear very similar except that the tissue below the bulbar conjunctiva observed in the nasal scans shows discrete peaks and valleys. The nasal scans of the limbus also show the termination of the corneal Descemet's-endothelium complex (Fig. 3E), which was not observed in the temporal scans due to the short scanning range of the UHROCT system (~1.3mm in air).

#143753 - $15.00 USD Received 7 Mar 2011; revised 27 May 2011; accepted 31 May 2011; published 1 Jun 2011

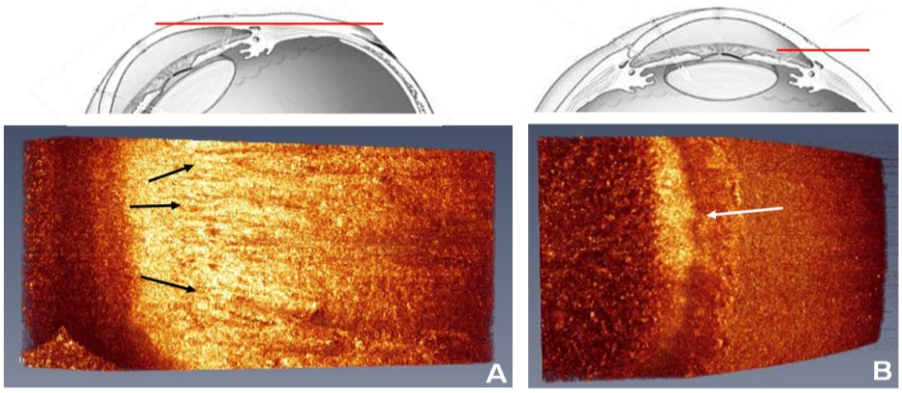

Fig. 4. Frames from movies (Media 1 and Media 2) based on volumetric temporal scans of the human limbus. Dimensions: 1000 x 350x256 (A-scans x pixels x B-scans). The orientation of the en-face sections form the 3D stack are marked with red lines in the human eye diagrams.

A series of three-dimensional scans (1000 x 1024 x 256) were also acquired from rectangular areas (~4mm x 2mm) of the limbus of each subject. Two movies, presented in Fig. 4 show in-depth, en-face views of the limbus in two different orientations: parallel to the limbus surface (A) and parallel to the pupil plane (B). The red lines in the human eye diagrams above the movie frames indicate the orientation of the en-face scans.

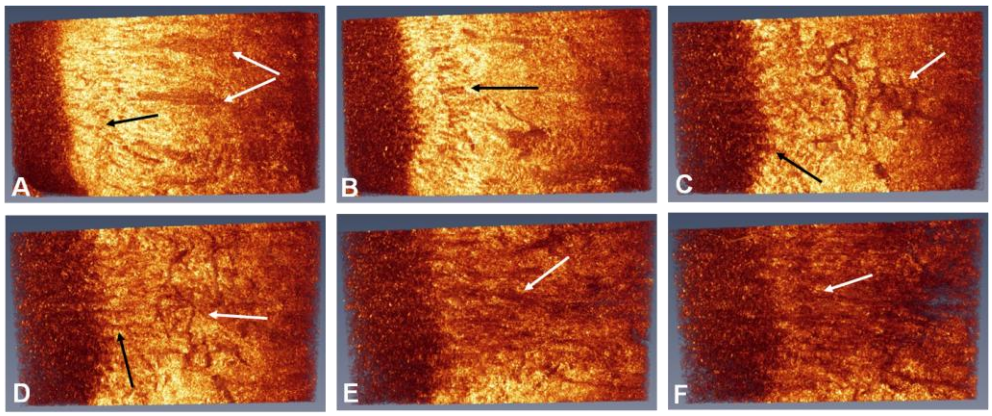

Fig. 5. Selected en-face frames from Media 1 (Fig. 4A). White arrows in (A) mark the low scattering locations in the limbus between the ridges of the Vogt palisades that house corneal stem cells. The black arrows in (A-D) mark a network of micro-channels that connect the cornea with the sclera at different depths in the limbus. In (C,D) white arrows mark the blood and lymph vessels in the sclera, while in (E,F) they point at channel like features connecting the cornea with the sclera that are most likely part of the trabecular meshwork.

The black arrows in the frame shown in Fig. 4A mark what appear to be the highly scattering collagen ridges of the Vogt palisades. The white arrow in the frame in Fig. 4B marks the transition from the corneal epithelium to the bulbar conjunctiva. Because the movies are rich in structural details, selected frames from the movie in Fig. 4A are shown in Fig. 5 to highlight and discuss specific morphological features. The left side of the images shows the corneal region, while the right side corresponds to the sclera.

Figure 5A shows an en-face scan acquired ~70 µm below the corneal/conjunctiva surface. Several elliptically shaped, low reflective structural features (white arrows) are observed in between the highly scattering collagen ridges of the putative Vogt palisades. By comparing the size (50µm to 200 µm in diameter, ~500 µm in length), location (50 µm to 100 µm below the tissue surface) and reduced scattering properties of these structures with similar morphological features observed in the limbus with LSCM [11] we can conclude that most

#143753 - $15.00 USD Received 7 Mar 2011; revised 27 May 2011; accepted 31 May 2011; published 1 Jun 2011

likely these features correspond to the locations in the Vogt palisades that house the stem cells responsible for the regeneration of the corneal epithelium. Because the stem cells have large cytoplasm-to-nucleus ratio, these regions appear less scattering in the OCT tomograms as compared to the fibrous ridges of the palisades.

A network of radially oriented, channel-like, low reflective features are observed at different depths in the limbus (black arrows, A-D), that appear to extend from the cornea toward the sclera. These channels appear to connect to the blood vasculature in the sclera (white arrows, C and D) at depths of 100 µm–150 µm below the tissue surface. The image frames E and F were acquired at depths of ~500µm below the tissue surface and show another set of channel like features that most likely are part of the trabecular meshwork or the drainage system. These channel-like structures bare close resemblance to the microchannels observed *in vivo* in the human limbus with LSCM [11].

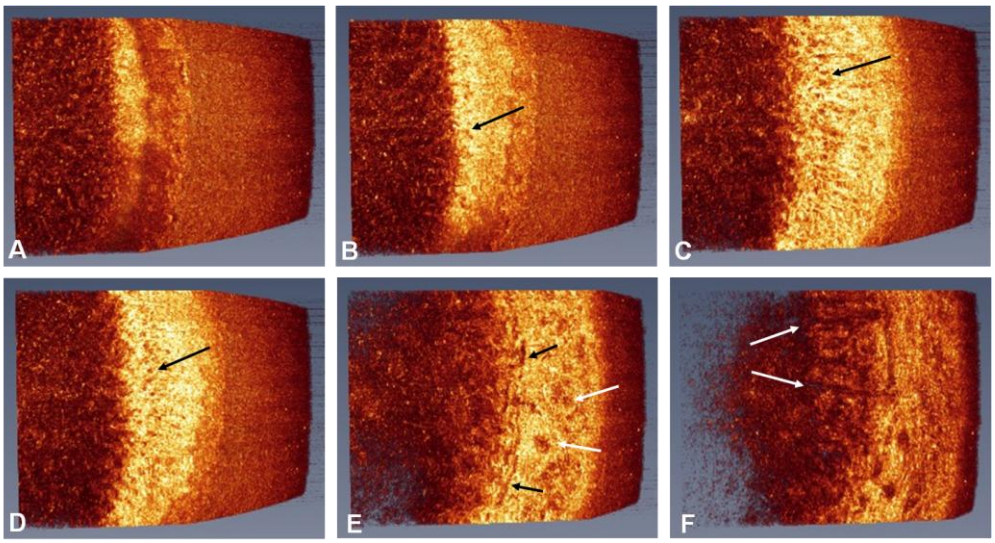

Fig. 6. Selected frames Media 2 (Fig. 4B). Black arrows (B-E) mark cross-sections of the micro-channels that extend from the cornea toward the sclera. White arrows mark cross-section of the blood and lymph vessels in the sclera (E) and the trabecular meshwork (F).

The images presented in Fig. 6 are selected frames from the movie in Fig. 4B, which is based on the same data set, with different orientation of the en-face cross-sections. The image in Fig. 6A was acquired at a depth ~50µm below the tissue surface and shows the transition between the cornea and the bulbar conjunctiva in the limbus (black arrow). The images in Fig. 6 B-D show the circular cross-sections (black arrows) of the micro-channels ~10-20µm in diameter, that extend from the cornea toward the sclera, at different imaging depths within the limbus. The larger circular features (~20-50µm in diameter) in Fig. 6E marked with white arrows and located within the highly scattering sclera are most likely cross-sections of the blood and lymph vessels. Smaller (~10-20µm in diameter) channel-like features were observed on the same frame closer to the cornea, forming what appears to be an arc from a circle (black arrows). Given the imaging depth (~500µm below the corneal surface), it is likely that these morphological features are elements of the aqueous humor drainage system. The image in Fig. 6F was acquired ~50µm deeper than the frame in Fig. 6E, and reveals both radial and arc channel-like features (white arrows), that could be parts of the trabecular meshwork.

4. Conclusion

We utilized a high speed, UHROCT system, operating in the 1060nm spectral region to image and identify structural details in the human limbus. The results acquired from healthy subjects

#143753 - $15.00 USD Received 7 Mar 2011; revised 27 May 2011; accepted 31 May 2011; published 1 Jun 2011

show that the imaging technology allows for *in vivo*, volumetric visualization of morphological features in the cornea, limbus and sclera that appear to be corneal nerve fibers, Vogt palisades, as well as blood and lymph vessels in the conjunctiva and sclera/episclera. This work is important for the clinical assessment of the structure and function of the normal human limbus. In addition, the benefit of high speed, cellular level, volumetric imaging of the limbus promises to have significant impact on the clinical visualization of diseases and surgery of this very sensitive region of the eye.

Acknowledgments

The authors would like to thank P. Lee, D. Lee, S. Shakeel and J. Maram for assistance with the data acquisition and processing. This work was supported in part by the Natural Sciences and Engineering Research Council of Canada (NSERC) and the Canadian Institute of Health Research (CIHR).

#143753 - $15.00 USD Received 7 Mar 2011; revised 27 May 2011; accepted 31 May 2011; published 1 Jun 2011